Turbulent Flow About Airfoils

SmartNumerics Simulation Solutions Inc.

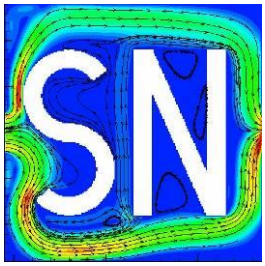

September 1, 2022

Table of Contents

1.0 Introduction

CFD codes are validated in part by comparing computed airfoil forces, pressure profiles, and friction profiles to data collected using airfoil wing models inserted in wind tunnels. The angle of attack used in the (typically) two-dimensional simulation must be made smaller than the experimental angle of attack (AOA) to adjust for the effect of the wind tunnel walls. The need to adjust AOA is mostly due to the effect of the top and bottom walls of the tunnel. In addition, some workers adjust the camber of the airfoil used in the simulation to compensate for the effects of the upper and lower walls. The tunnel side walls also effect the measurement due to the presence the side-wall boundary layers. These boundary layers reduce flow near the walls and increase it outside of the boundary layers. The ratio of the wingspan to chord must be large enough so that measurements taken at midspan are not appreciably affected by the side wall boundary layers. The simulation may match experiment more closely if the flow speed is slightly increased.

The degree of agreement between the 2D simulation with adjusted AOA and Mach number and the 3D experiment, is used as a measure of the suitability of the turbulence model being used. Different turbulence models require slightly different values of adjusted AOA to obtain the best match to experiment. The most suitable turbulence model will produce the best match to lift, drag, Cp curves, C_f curves, and shock location.

The same turbulence model implemented by different authors may require different values of adjusted AOA and flow velocity to match experiment. The turbulence model may be implemented in slightly different ways. The details of the flux calculation including the spatial accuracy and choice of limiter function can affect the drag and thus the optimal AOA. The simulations typically match experimental pressures reasonably well along the underside of the airfoil. With AOA adjusted to match experimental shock location, the pressures along the top of the airfoil matches experiment reasonably well upstream of the shock except for leading edge where turbulence models generally do not model transition from laminar flow to turbulent flow.

2.0 Simulation of Attached Turbulent Flow about RAE 2822 Airfoil

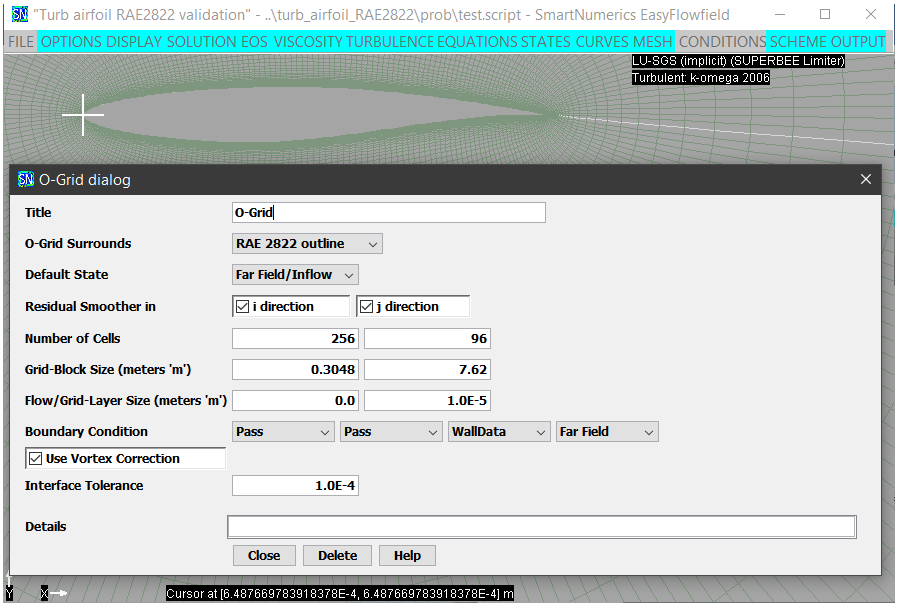

Fig. 1: Grid used to simulate turbulent flow about the RAE 2822 airfoil (case 6).

Figure 1 displays the parameters used to generate a 256x96 cell grid about the RAE 2822 airfoil. A no-slip boundary condition was imposed at the surface of the airfoil. A vortex correction was used at the far-field boundary which was approximately 25 chords from the airfoil.

Cook, McDonald, and Firmin [1] performed a series of turbulent tests in a wind tunnel using the RAE 2822 airfoil. These tests have been used as the basis of simulations by various workers. See, for example, Holst [2]. The following simulation is based on transonic case 6 of Cook, McDonald, and Firmin [1]. The specified experimental conditions were Mach 0.725, angle of attack 2.92°, and Reynolds number of 6.5×10^6 based on airfoil chord. The coefficients of lift, drag, and pitching moment from the experiment were 0.743, 0.0127, and -0.095, respectively.

The simulation was performed with a far-field Mach number of 0.729 with the angle of attack set to 2.31° to adjust for the influence of the wind tunnel walls. The Reynolds number based on a chord of one foot was 6.5×10^6. These conditions were taken from the RAE 2822 validation test in the NPARC alliance validation archive. The far-field turbulence intensity was set to 0.5% and the far-field eddy viscosity was one-tenth of the laminar viscosity. The aerodynamic center was set to the quarter chord point.

An (implicit) LU-SGS solver was used with a CFL number of 400. The SUPERBEE limiter was used with the compression parameter set to 1.48 to obtain a thinner shock front and lower drag than achievable using the van Albada limiter. The solution is second order accurate in space except near the shock front. The k-ω 2006 model of Wilcox [3] was used without a wall function. The result of a steady-state simulation performed on a 128x96 cell grid was transferred to the 256x96 cell grid after 3,500 cycles and the simulation was continued for an additional 2,500 cycles with a CFL number of 800.

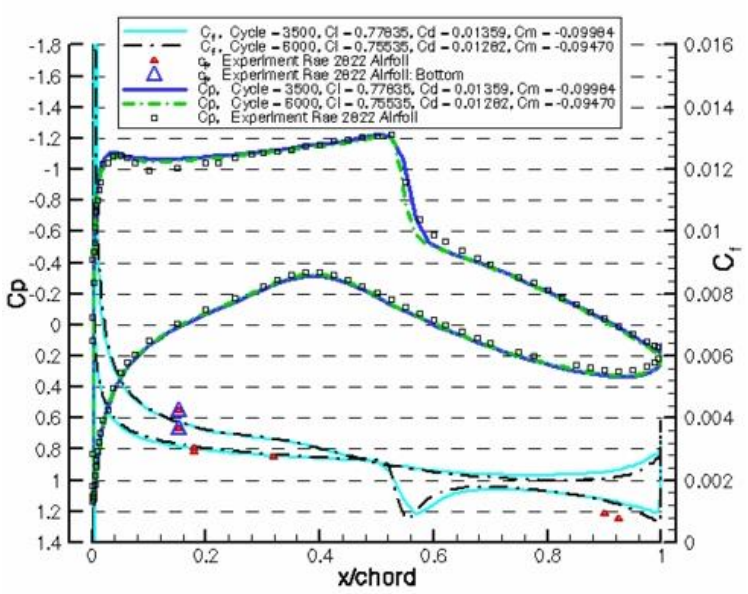

Fig. 2a: Case 6 pressure & friction for flow about RAE 2822 airfoil (k-ω 2006).

In Figure 2a, the Cp and C_f curves are in good agreement with the experimental values. The final coefficients of lift, drag, and pitching moment are respectively within 1.7%, 0.95%, and 0.32% of the experimental values. The final values of y^+ based on cell height next to the airfoil vary from 0.56 to 0.0075. Similar results are obtained with the far-field turbulence intensity set to 0.05%.

The pressure coefficient from the simulation is computed using

$$c_p = \frac{p_w - p_\infty}{\frac{1}{2}\rho_\infty U_\infty^2}$$

where p_w is the local pressure at the wall, p_∞ is the far-field pressure, ρ_∞ is the far-field density, and U_∞ is the far-field velocity. Also displayed are the skin friction coefficients computed using

$$c_f = \frac{\rho_w (u^*)^2}{\frac{\gamma}{2} p_w M_{is}^2} sign(u^*)$$

where u^* is the local friction velocity output by the solver, ρ_w is the local density at the wall, and the denominator is an approximation to the dynamic pressure at the edge of the boundary layer. Here γ is the specific heat ratio and

$$M_{is} = \sqrt{\frac{2}{\gamma - 1}\left(\left(\frac{P_{tot}^\infty}{p_w}\right)^{(\gamma-1)/\gamma} - 1\right)}^{1/2}$$

is the isentropic Mach number where P_{tot}^∞ is the freestream total pressure. Unlike the far-field dynamic pressure used in the denominator for *Cp*, the dynamic pressure at the edge of the boundary layer varies along the airfoil. According to Holst [2], the experimental values of friction were referenced to the dynamic pressure at the edge of the boundary layer. The friction velocity is output with a negative sign if the flow along the wall is reversed. Thus, the plotted friction is negative where the flow reverses. The flow

remains attached in this case. There is no reversal of flow seen in the simulation or in the experiment. Figure 2b displays contours of Mach number.

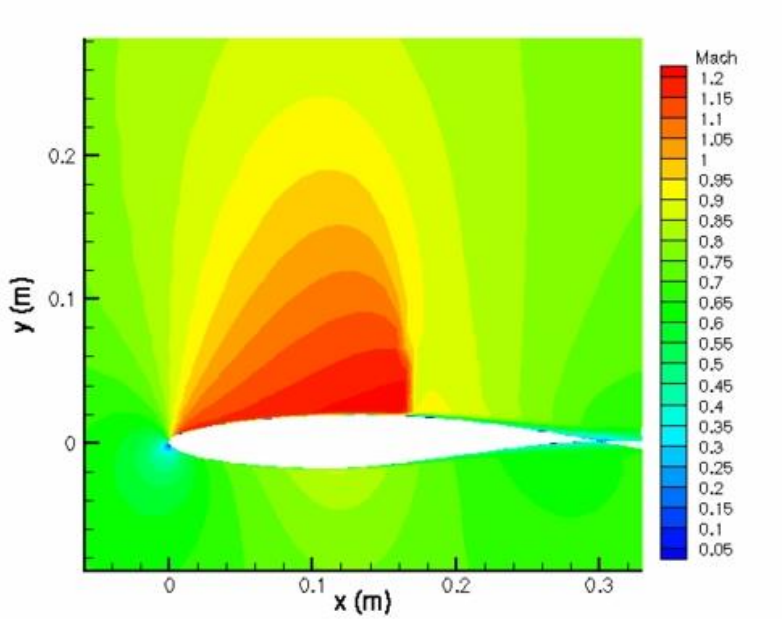

Fig. 2b: Case 6 Mach contours at 7,000 cycles for flow about RAE 2822l (k-ω 2006).

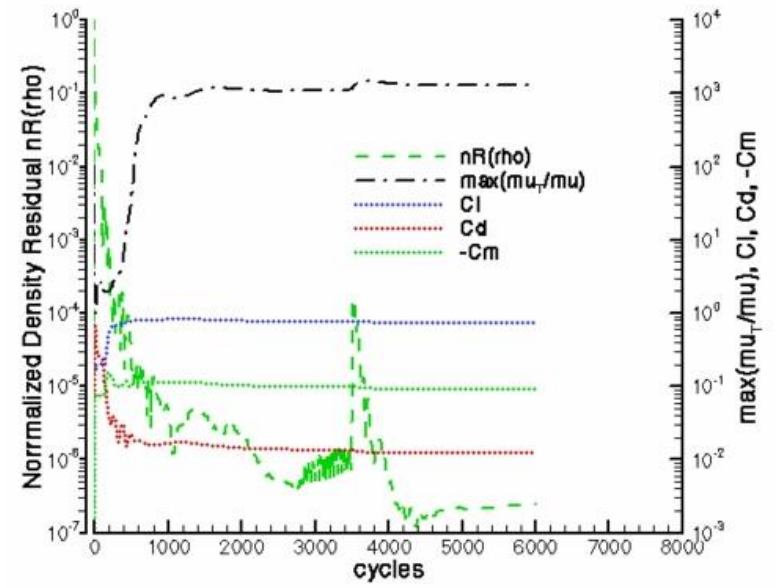

Fig. 2c: Case 6 convergence history for flow about RAE 2822 airfoil (k-ω 2006).

In Figure 2c, max(mu_T/mu) is a plot of the maximum ratio of eddy viscosity (μ_T) to molecular viscosity (μ). This ratio and the force coefficients C_l, C_d, and C_m approach constant values as the steady state is reached on a particular grid. The RMS average of the density residual is normalized by the maximum RMS value computed during the first few cycles.

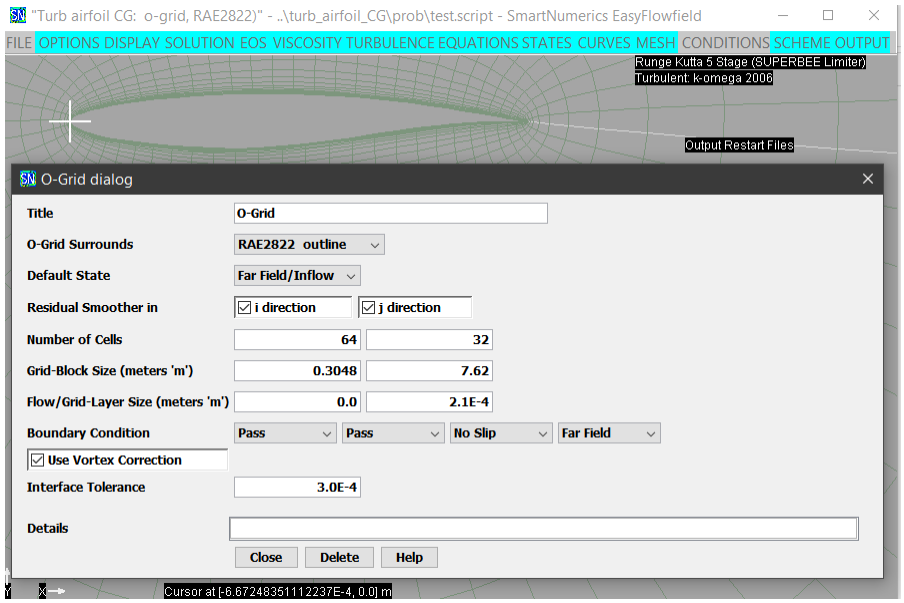

Fig. 3: Grid used to simulate flow about the RAE 2822 (case 6, with wall function).

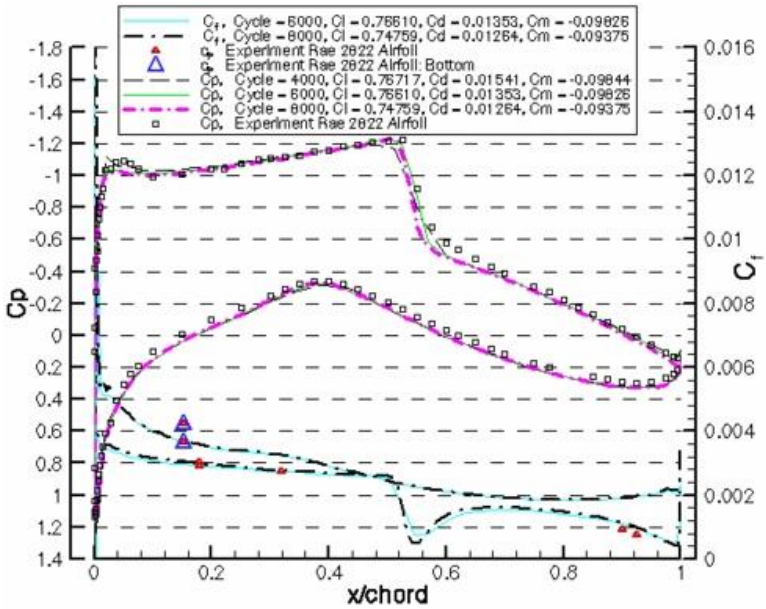

Fig. 4a: Case 6 pressure and friction for flow about RAE 2822 (k-ω 2006, wall func.).

The simulation was also performed on a somewhat coarser grid using an automatic (adaptive) wall function and an (explicit) five-stage Runge-Kutta solver with a CFL number per stage of 0.45. The SUPERBEE limiter was used with the compression parameter set to 1.47. When using an explicit solver, the SUPERBEE limiter produces a larger final residual than can be obtained using the van Albada limiter but results in a more accurate solution. The initial simulation on a 64x32 cell grid displayed in Figure 3 was transferred to a 128x32 cell grid and then to a 256x32 cell grid.

The solution curves and convergence history are displayed in Figures 4a and 4b. The final coefficients of lift, drag, and pitching moment are respectively within 0.62%, 0.47%, and 1.3% of the experimental values. The final values of y^+ based on cell height next to the airfoil vary from 31 to 0.41. Similar results are obtained with the far-field turbulence intensity set to 0.05%.

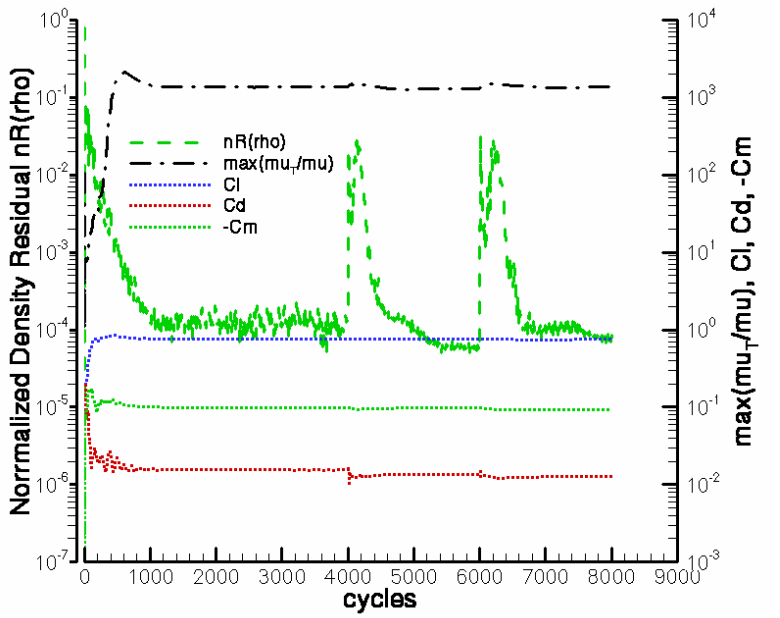

Fig. 4b: Case 6 convergence history for flow about RAE 2822 (k-ω 2006, wall func.).

Figures 5a and 5b display the results of repeating the simulation using the preconditioned LU-SGS scheme. The simulation starts at an initial CFL of 0.45 which is gradually increased by a factor of five after a delay of 500 cycles. All other parameters are unchanged. The final coefficients of lift, drag, and pitching moment are respectively within 0.27%, 1.0%, and 1.9% of the experimental values. The final values of y^+ based on cell height next to the airfoil vary from 31 to 0.35.

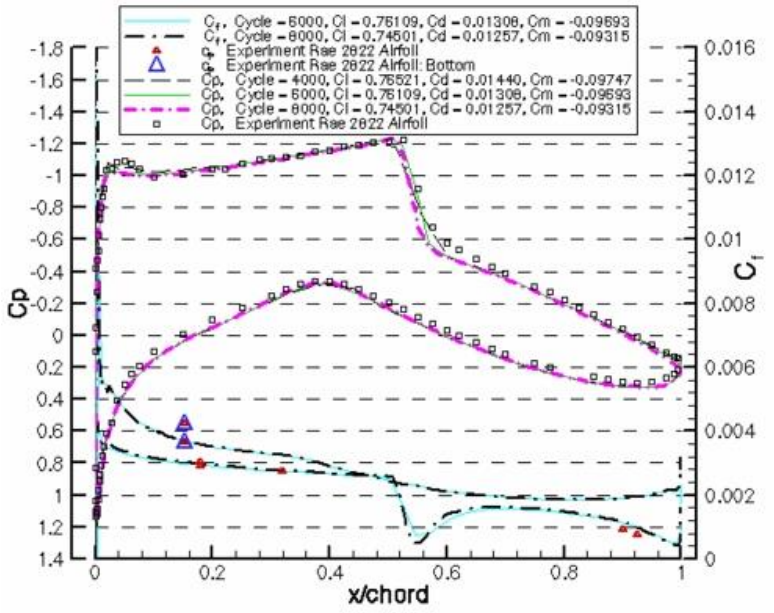

Fig. 5a: Case 6 pressure and friction for flow about RAE 2822 (k-ω 2006, wall func., IMPL).

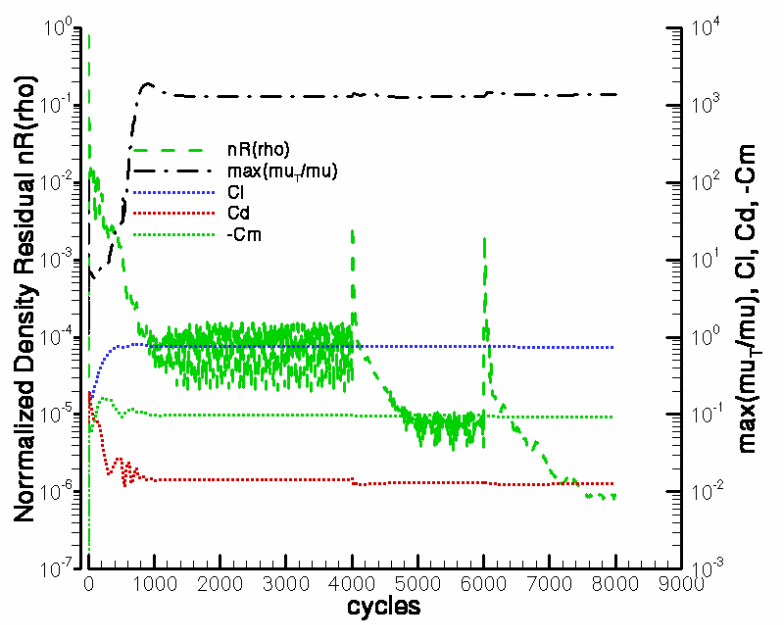

Fig. 5b: Case 6 convergence history for flow about RAE 2822 (k-ω 2006, wall func., IMPL).

3.0 Simulation of Detached Turbulent Flow about RAE 2822 Airfoil

According to Holst [2], case 10 of Cook, McDonald, and Firmin [1] is a much more difficult test of a turbulence model than case 6. Unlike case 6, significant boundary layer separation occurs downstream of the shock. The specified experimental conditions are Mach 0.75, angle of attack 3.19°, and Reynolds number of 6.2×10^6 based on airfoil chord. The experimental coefficients of lift and drag, and pitching moment are 0.742, 0.0242, and -0.106 respectively.

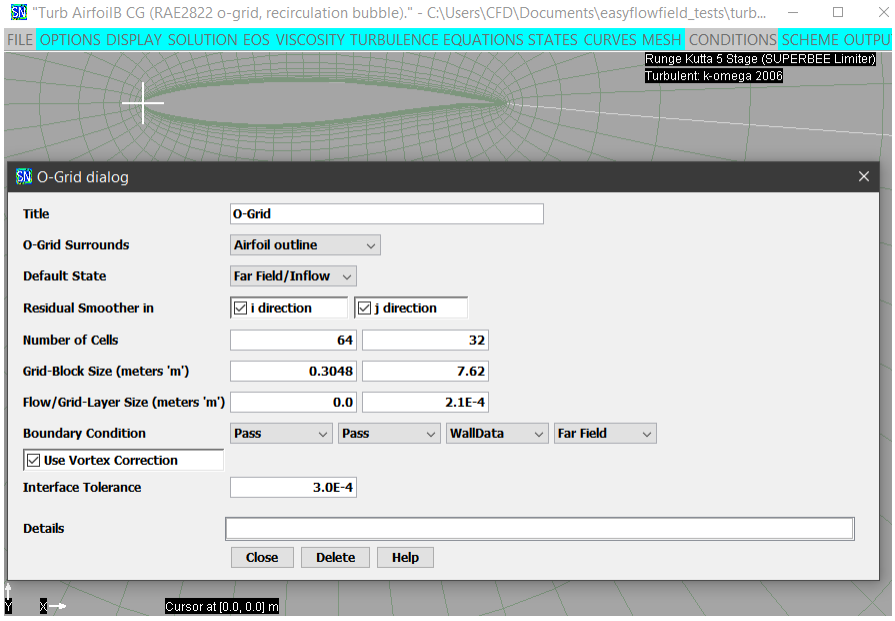

Fig. 6: Grid used to simulate flow about the RAE 2822 airfoil (case 10, wall func.).

Figure 6 displays the parameters used to generate an o-grid about the RAE 2822 airfoil for use with the automatic wall function.

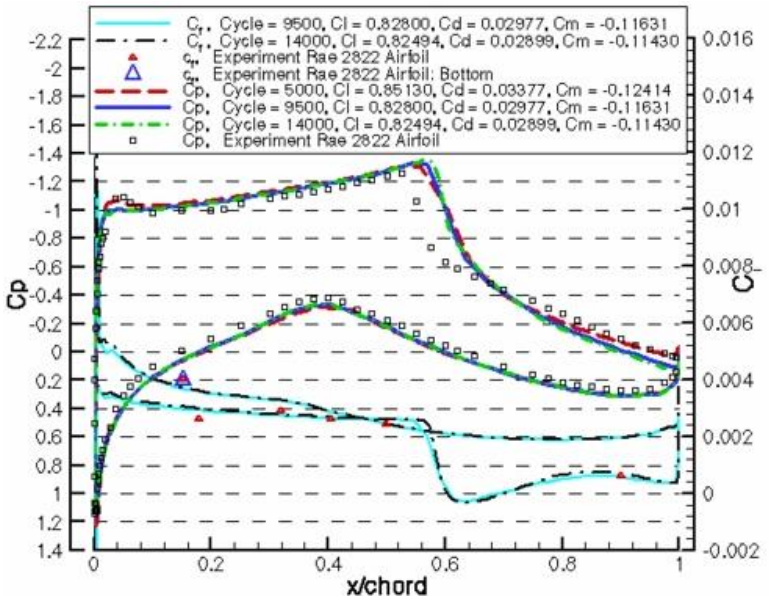

Fig. 7a: Case 10 pressure & friction for flow about RAE 2822 (k-ω 2006, wall func.).

After Bardina, Huang, and Coakley [4], the simulation was performed with a far-field Mach number of 0.75 with the angle of attack set to 2.79°. The Reynolds number based on a chord of one foot was 6.2×10^6. The SUPERBEE limiter was used with the compression parameter set to 1.47. The five-stage Runge-Kutta solver was used with a CFL number of 0.52. The aerodynamic center was set to the quarter chord point.

Figures 7a through 7c display the solution using the k-ω 2006 turbulence model. The location of shock front is somewhat downstream of the experimental location. This is typical of most published results for the simulation of case 10 using a variety of two-equation turbulence models with and without use of a wall function. However, the friction curves are in reasonable agreement with experiment and reveal a region of flow separation where the friction coefficient is negative. The final coefficients of lift, drag, and pitching moment are respectively within 11%, 20%, and 7.8% of the experimental values. The final values of y^+ based on cell height next to the airfoil vary from 29 to 0.43.

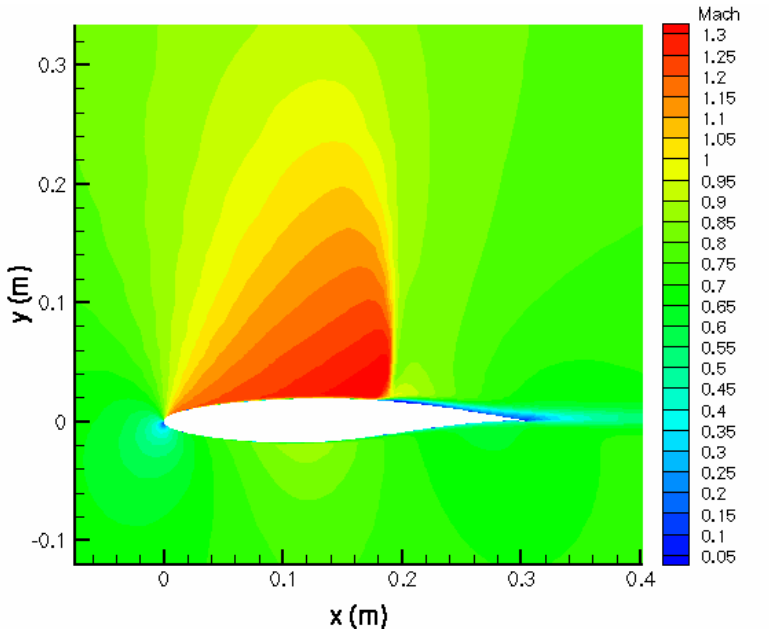

Fig. 7b: Case 10 Mach contours for flow about RAE 2822 (k-ω 2006, wall func.).

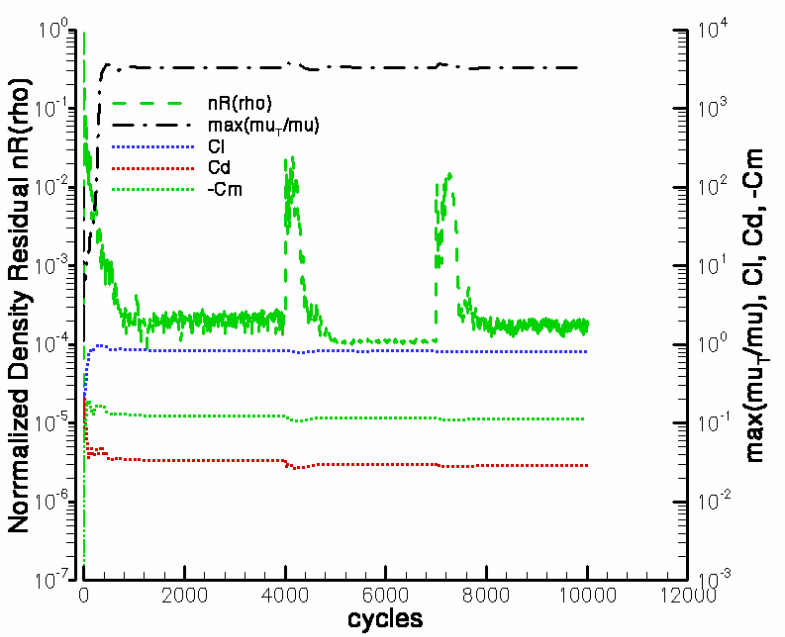

Fig. 7c: Case 10 convergence history for flow about RAE 2822 (k-ω 2006, wall func.).

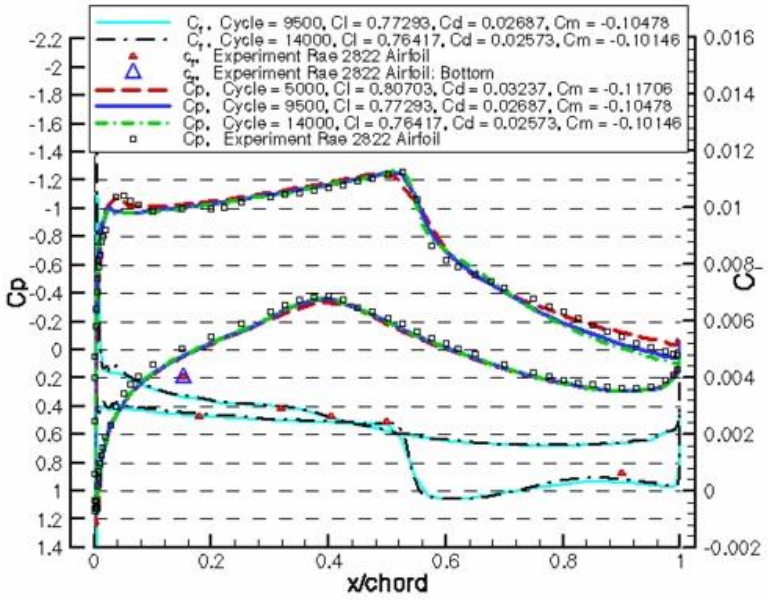

Fig. 8a: Case 10 pressure & friction for RAE 2822 (k-ω 2006, Lim = 1.1, wall func.).

Figures 8a through 8c display the solution with the stress limiter weight in the k-ω 2006 turbulence model increased from the standard value of 0.875 to 1.1. The SUPERBEE limiter is used with the compression parameter set to 1.47. The five-stage Runge-Kutta solver is used with a CFL number of 0.52. The location of the shock front from the simulation is much closer to the experimental location. The region of flow separation is also further upstream. Use of the higher stress limit required additional cycles to reach the steady state. The final coefficients of lift, drag, and pitching moment are respectively within 3.0%, 6.3%, and 4.3% of the experimental values. The final values of y^+ based on cell height next to the airfoil vary from 28 to 0.46.

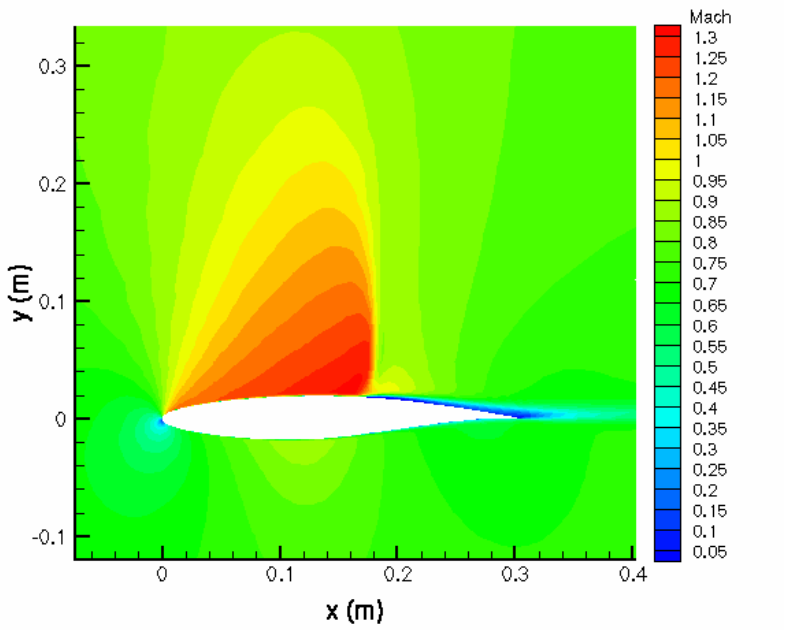

Fig. 8b: Case 10 Mach contours for RAE 2822 (k-ω 2006, Lim =1.1, wall func.).

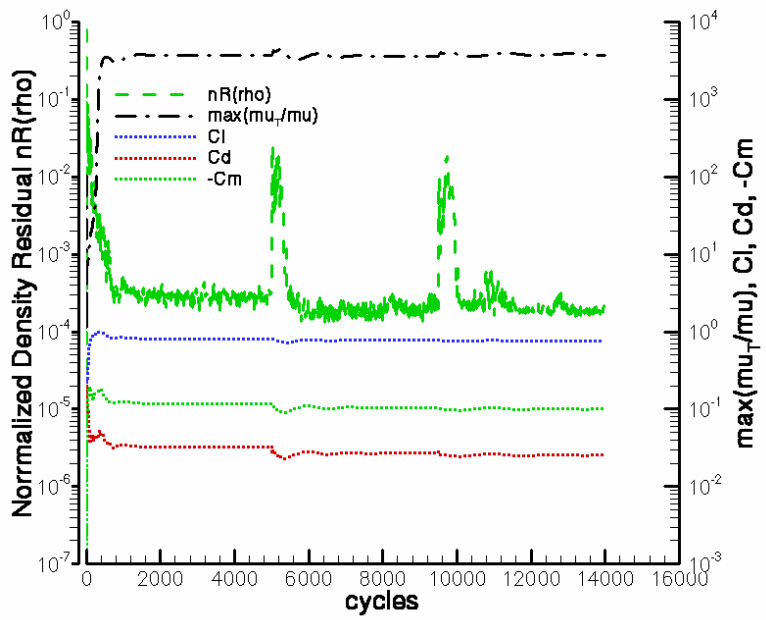

Fig. 8c: Case 10 convergence history for RAE 2822 (k-ω 2006, Lim = 1.1, wall func.).

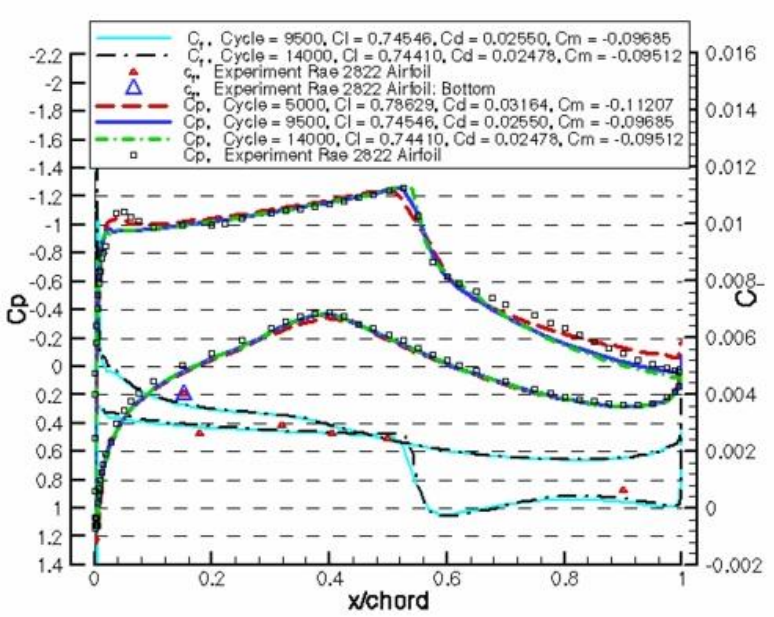

Fig. 9a: Case 10 pressure & friction for flow about RAE 2822 (SST 0.227, wall func.).

Figures 9a through 9c display the solution with the stress-limiter coefficient in the SST turbulence model of Menter [5] decreased from the standard value of 0.31 to 0.227. The SUPERBEE limiter is used with the compression parameter set to 1.47. The five-stage Runge-Kutta solver is used with a CFL number of 0.45. The final coefficients of lift, drag, and pitching moment are respectively within 0.28%, 2.4%, and 10% of the experimental values. The final values of y^+ based on cell height next to the airfoil vary from 29 to 0.47. The is no visible difference in the solution curves if a far-field turbulence intensity of 0.05% is used instead of 0.5%. The small oscillations seen in the k-ω 2006 solution are not present in the SST solution.

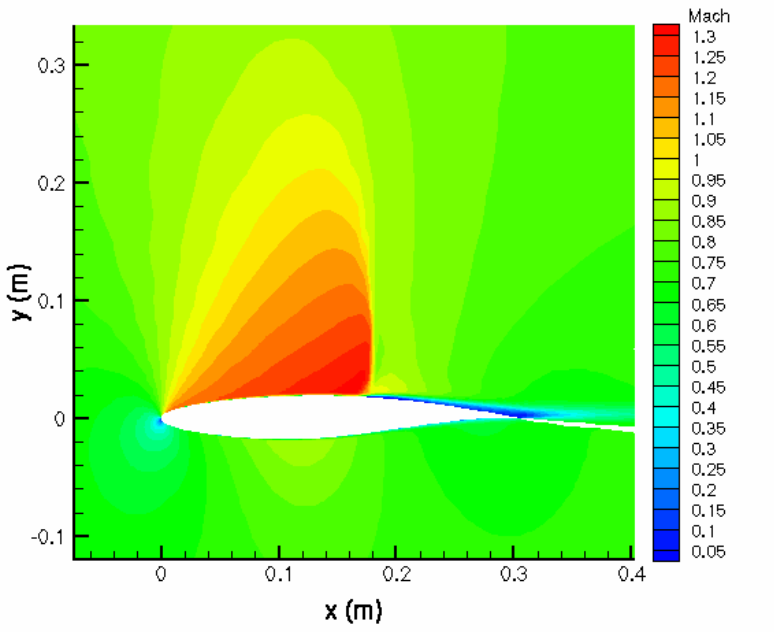

Fig. 9b: Case 10 Mach contours for flow about RAE 2822 (SST 0.227, wall function).

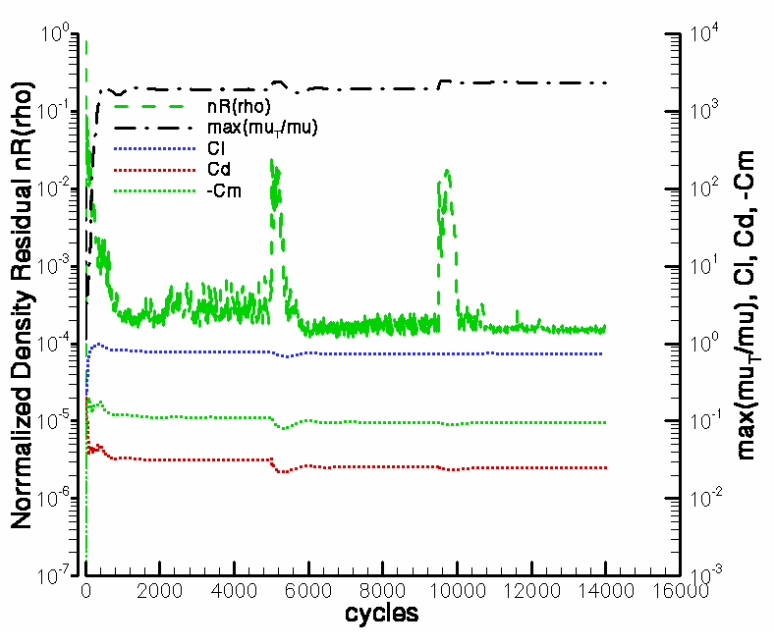

Fig. 9c: Case 10 convergence for flow about RAE 2822 (SST 0.227, wall func.).

Figures 10a and 10b display the results of repeating the simulation using the preconditioned LU-SGS scheme. The simulation starts at an initial CFL of 0.4 which is gradually increased by a factor of five after a delay of 500 cycles. All other parameters are unchanged. The final coefficients of lift, drag, and pitching moment are respectively within 0.04%, 2.1%, and 11% of the experimental values. The final values of y^+ based on cell height next to the airfoil vary from 29 to 0.41.

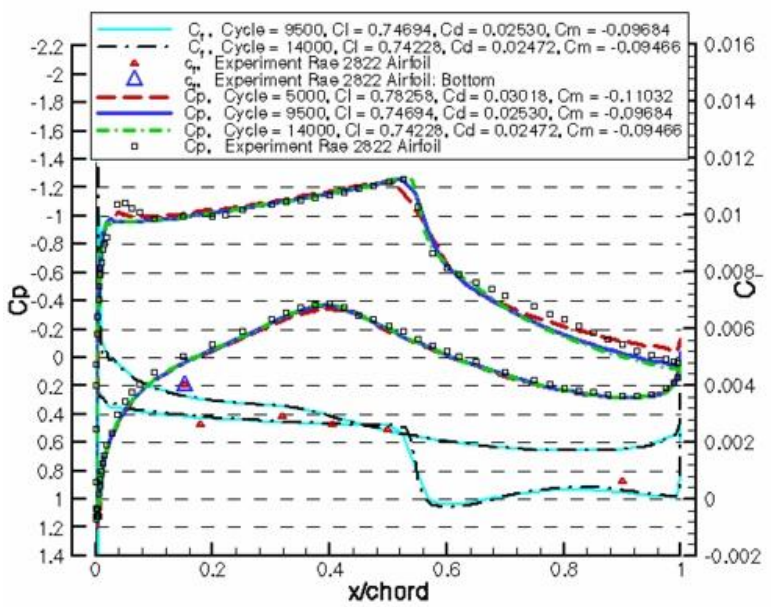

Fig. 10a: Case 10 pressure & friction for flow about RAE 2822 (SST 0.227, wall func., IMPL).

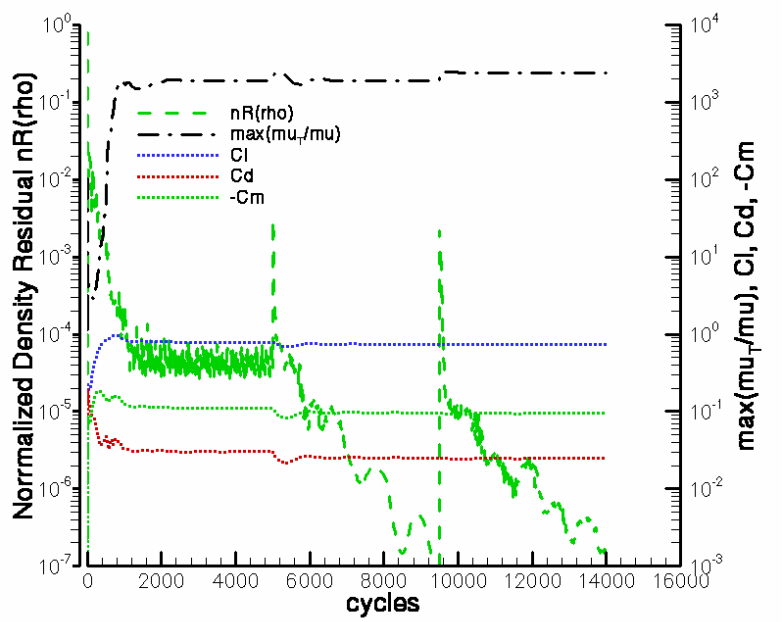

Fig. 10b: Case 10 convergence for flow about RAE 2822 (SST 0.227, wall func., IMPL).

4.0 Drag versus AOA for Turbulent Flow about NACA 0012 Airfoil

This validation test case is based on the experimental work of Ladson [5]. The measurements were performed in the NASA Langley Low-turbulence pressure tunnel. This wind tunnel was capable of running at total pressures ranging from 1 to 10 atmospheres. The test section was 36 inches in width and 90 inches in height. The airfoil model had a span of 36 inches and a chord of 23.66 inches. Experiments were performed at Reynolds Numbers based on chord ranging from $2x10^6$ to $12x10^6$. Various tests with and without tripping were performed at Mach numbers 0.05, 0.1, 0.15, 0.2, 0.25, 0.3, and 0.36. Tripping to force transition from laminar to turbulent flow was performed using carborundum sandpaper strips with grit sizes of 60, 80, 120, or 180. The tests without tripping gave lower values of drag. The turbulent intensity was not measured but was claimed to be quite low. The published force coefficients Cl, Cd, and Cm were corrected for the influence of the tunnel walls.

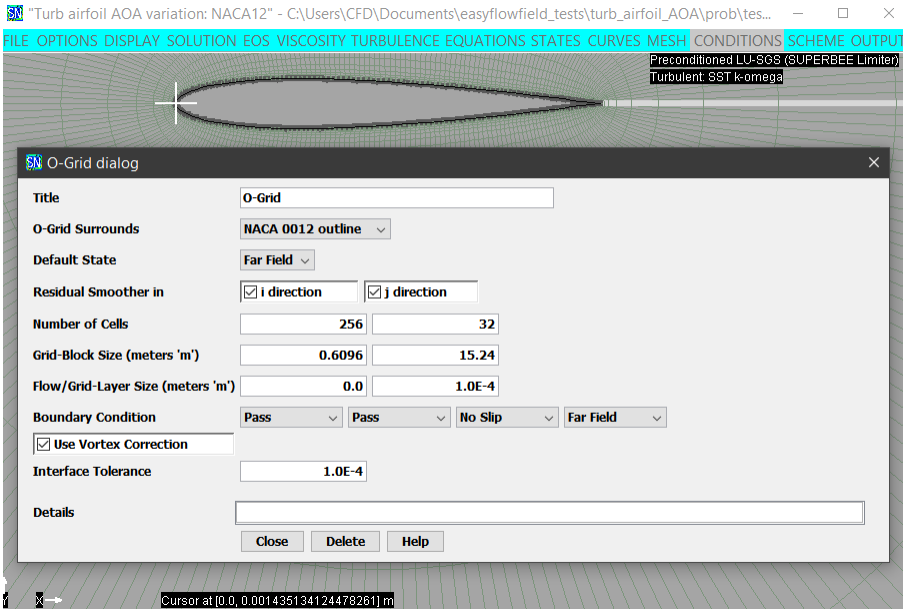

Fig. 11: Grid to simulate turbulent flow about NACA 0012 airfoil using wall function.

Turbulent flow about the NACA 0012 airfoil was modeled using the SST turbulence model with an automatic (adaptive) wall function. As in the previous section, the stress-limiter coefficient in the SST turbulence model was decreased from the standard value of 0.31 to 0.227. The far-field Mach number was 0.15 and the Reynolds number based on a chord of 2 feet was $6x10^6$. The preconditioned LU-SGS solver was used with an initial CFL of 0.45 which was gradually increased by a factor of five after a delay of 500 cycles. The SUPERBEE limiter was used with the compression parameter set to 1.47. The far-field turbulence intensity was set to 0.05% and the far-field eddy viscosity was one tenth of the molecular viscosity.

Figure 11 displays the parameters used to generate an o-grid about the NACA 0012 airfoil. The chord is set to 0.6096 m (2 feet), the far-field distance is 15.24 m, and the vertical grid-layer size is 10^{-4} m. The simulation is run at an initial angle of attack (AOA) of 0 degrees for 3,000 cycles. The AOA is subsequently increased by one degree every 3,000 cycles until an AOA of 24 degrees is reached. The final values of y^+ based on cell height next to the airfoil at an AOA of 24 vary from 8.6 to 0.11.

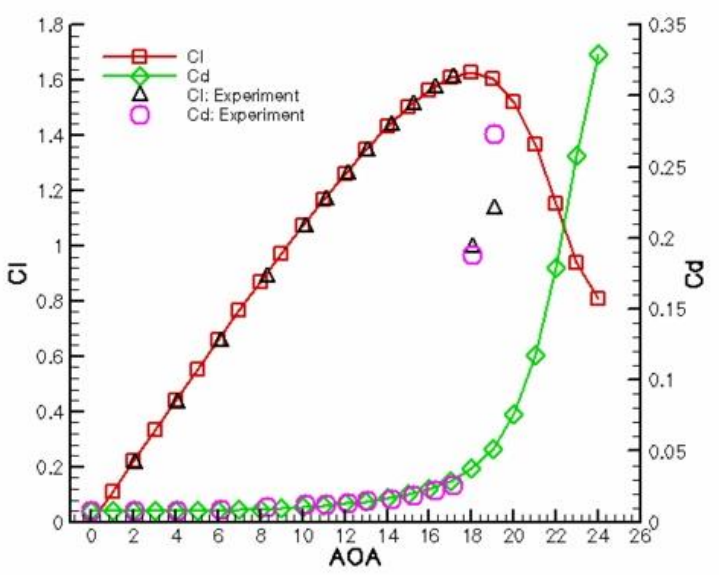

Fig. 12a: Lift & drag versus AOA (SST 0.227, SUPERBEE 1.47, auto, 256x32).

In Figure 12a, the lift and drag coefficients from the simulation are compared to experimental data from Ladson [5]. The lift coefficients from the simulation increase until the AOA reaches 18 degrees and then decreases as AOA continues to increase. The experimental angle of stall is near 17 degrees AOA and the drop in lift is much more severe than in the simulation. Drag is within 7% of experiment at 0 degrees AOA and within 10% at 16 degrees AOA. Detached flow occurs at high values of AOA and is seen in the simulation. Almost identical results are obtained if the turbulence intensity is increased from 0.05% to 0.5%. Halving or doubling the value of vertical grid-layer size reduces the fit to experiment for high values of AOA below 18 degrees.

The data from Ladson [5] was obtained with transition tripped at 5% of chord. As pointed out in the NASA code validation web page at https://turbmodels.larc.nasa.gov/naca0012_val.html, a turbulence model based on fully turbulent flow should be validated using experimental data with tripping. Figure 12b displays a plot of lift versus drag.

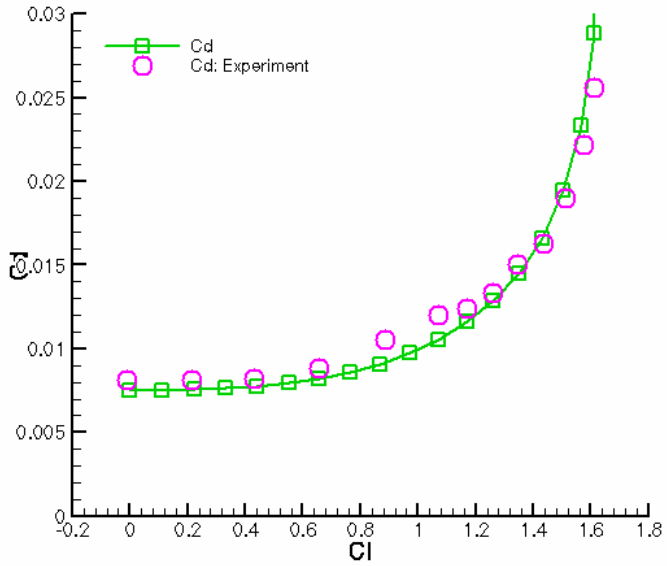

Fig. 12b: Drag versus lift (SST 0.227, SUPERBEE 1.47, auto, 256x32).

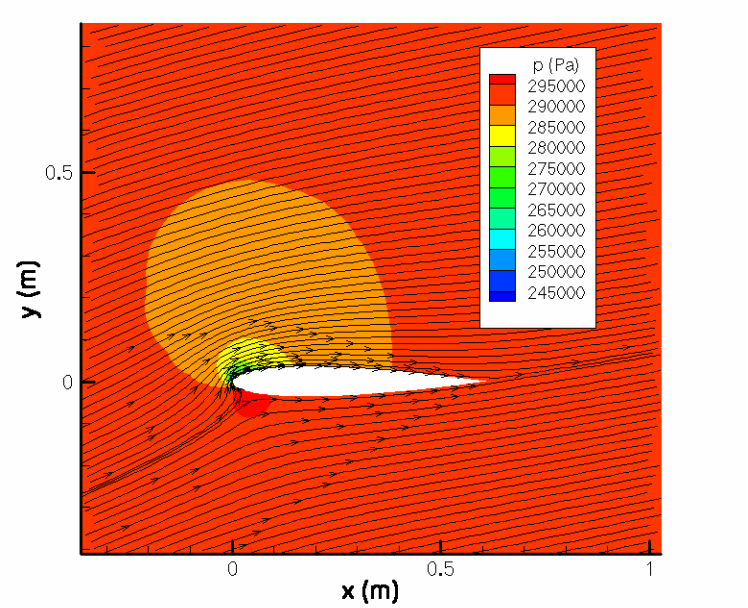

Fig. 12c: Pressure contours and streamlines at AOA of 15.

Figure 12c displays pressure contours and streamlines at 15 degrees AOA. There is a region of reverse flow on the underside of the airfoil where the flow spits to go around each side of the airfoil.

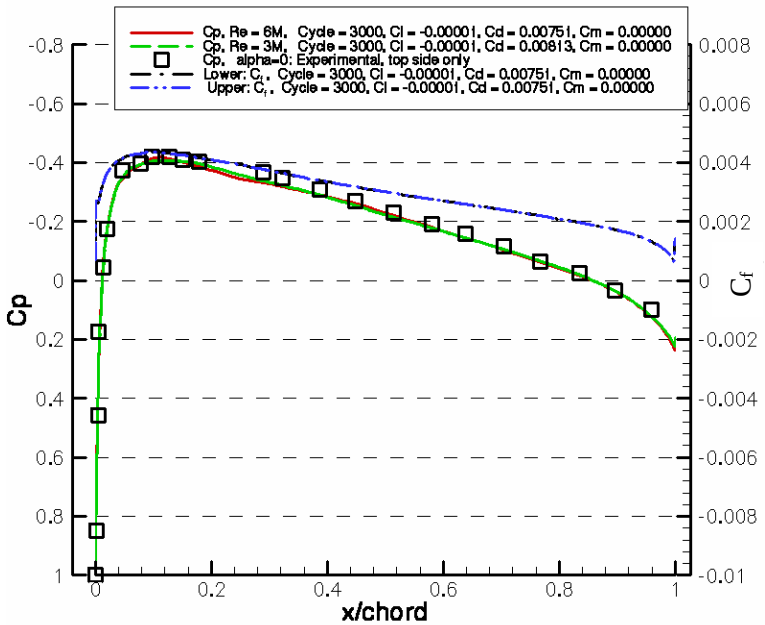

Fig. 12d: Cp and friction at AOA of 0 (SST 0.227, SUPERBEE 1.47, auto, 256x32).

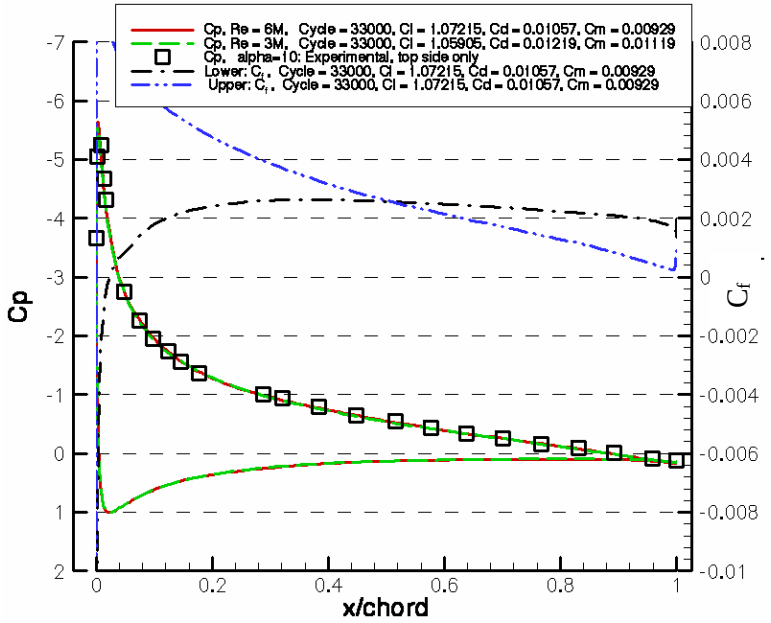

Fig. 12e: Cp and friction at AOA of 10 (SST 0.227, SUPERBEE 1.47, auto, 256x32).

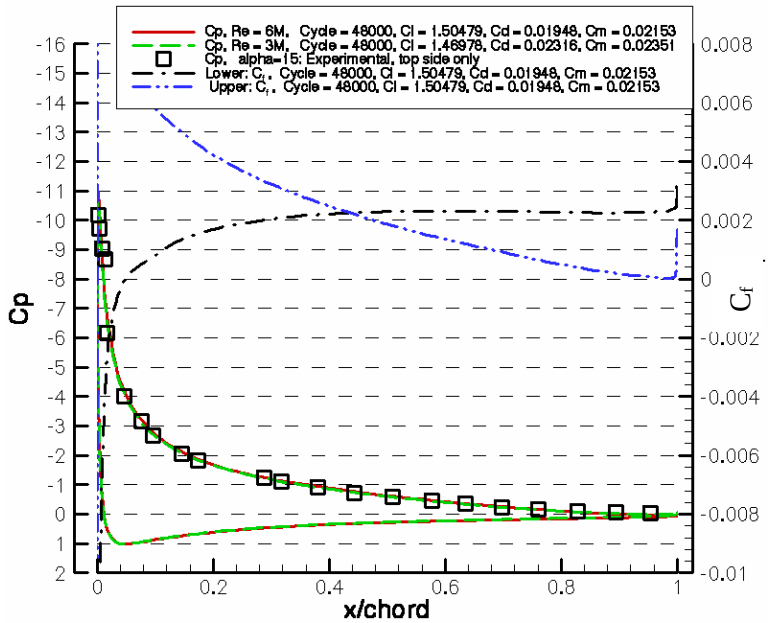

Fig. 12f: Cp and friction at AOA of 15 (SST 0.227, SUPERBEE 1.47, auto, 256x32).

Figures 12d through 12f display plots of the pressure coefficient along the airfoil from simulation compared to experimental values. The simulation using a Reynolds number of 3×10^6 (based on a chord of 1 foot) results in almost identical pressure coefficients but lower lift and higher drag. The original chord, far-field distance, and vertical grid-layer size were halved for this simulation. The ratio of the vertical grid-layer size to the chord thus remains unchanged. The friction coefficients from the simulation computed using

$$c_f = \frac{\rho_w (u^*)^2}{\frac{1}{2}\rho_\infty U_\infty^2} sign(u^*)$$

are also displayed.

As documented in the NASA website, the Cp values near the leading edge from Ladson [5] were insufficiently resolved for comparison to the values obtained from the simulations. The Cp values were instead taken from Gregory and O'Reilly [6]. These measurements were performed using the United Kingdom National Physical Laboratory 13 foot by 9-foot low speed wind tunnel. The Mach number was 0.16 (55 m/s) and the Reynolds number based on airfoil chord was 2.88×10^6. The airfoil model had a chord of 30 inches and a span of 9 feet. Turbulent flow was tripped on the airfoil by using bands of roughness stretching from the leading edge to 2.5% of chord on the upper surface and stretching from the leading edge to 10% of chord on the lower surface.

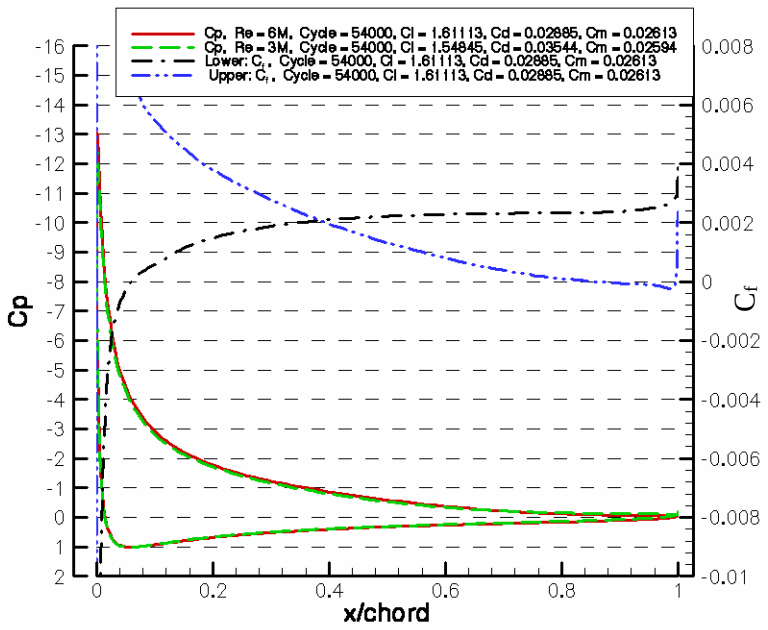

Fig. 12g: Cp and friction at AOA of 17 (SST 0.227, SUPERBEE 1.47, auto, 256x32).

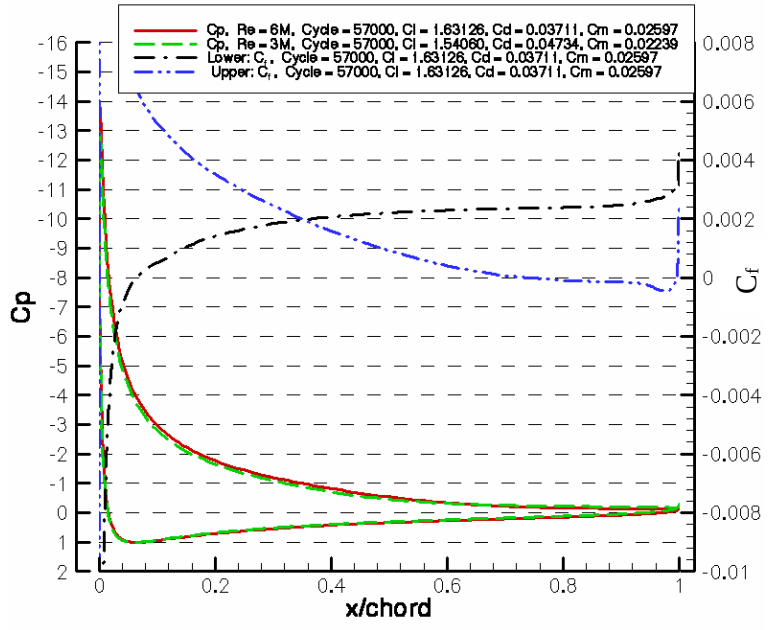

Fig. 12h: Cp and friction at AOA of 18 (SST 0.227, SUPERBEE 1.47, auto, 256x32).

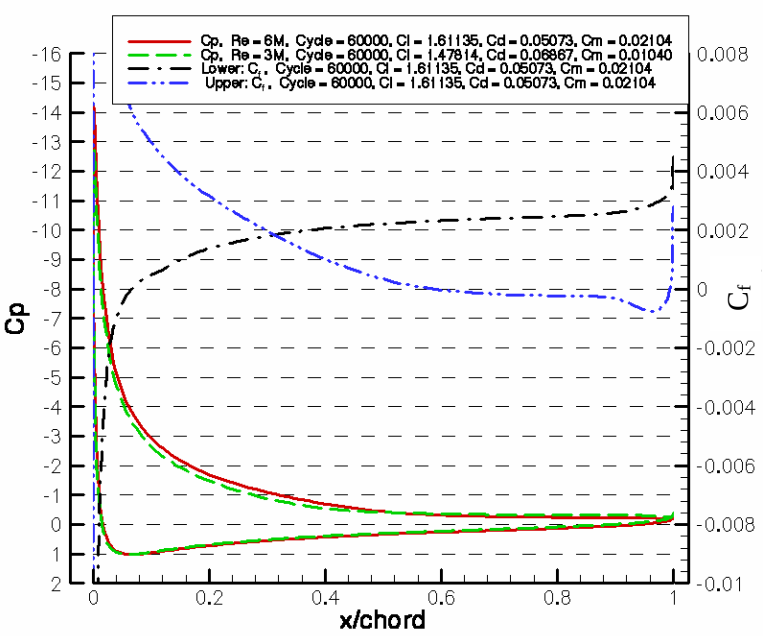

Fig. 12i: Cp and friction at AOA of 19 (SST 0.227, SUPERBEE 1.47, auto, 256x32).

Figures 12g through 12h display the pressure and friction coefficients near the stall angle. A small region of flow separation at 17 degrees AOA grows rapidly as AOA increases.

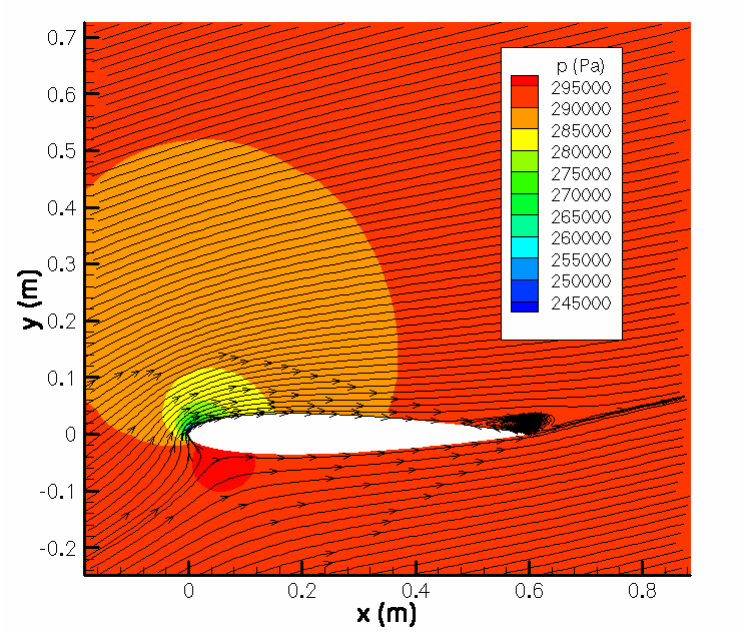

Fig. 12j: Pressure contours and streamlines at AOA of 18.

Figure 12j displays pressure contours and streamlines at 18 degrees AOA. There is a region of reverse flow on the underside of the airfoil were the flow spits to go around each side of the airfoil. The streamlines also show the region of recirculation and flow separation near the top trailing edge.

The simulation was repeated using a 512x32 grid and resulted in the same stall angle and a similar fit to experiment. A simulation using a 128x32 cell grid resulted in a stall angle near 16.5 degrees AOA and a poor fit to experimental values of lift and drag.

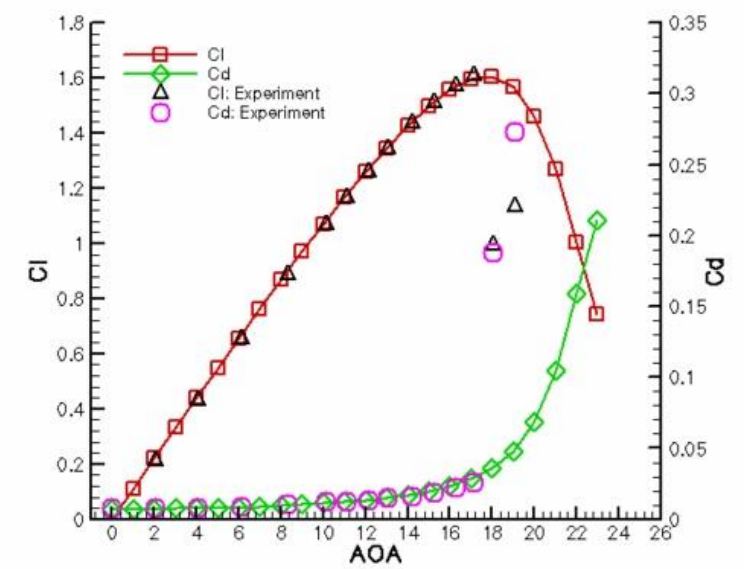

Fig. 13a: Lift & drag vs AOA (k-ω 2006, Lim = 1.1, SUPERBEE 1.47, auto, 256x32).

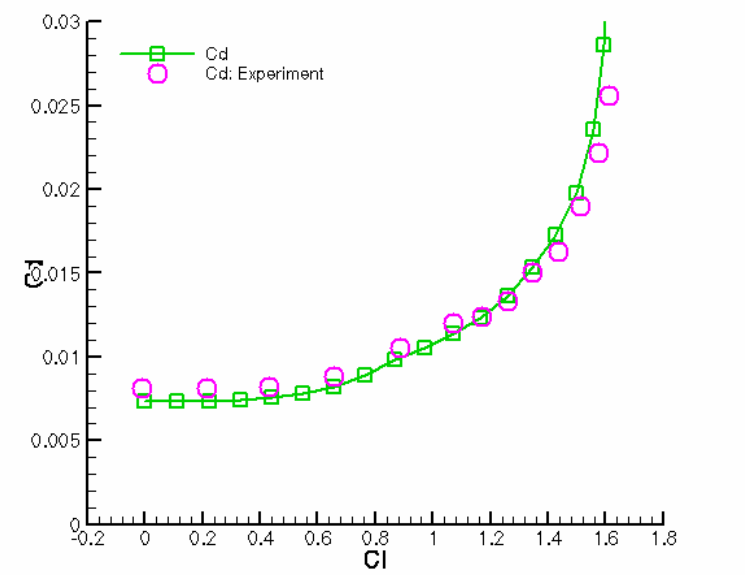

Fig. 13b: Drag versus lift (k-ω 2006, Lim = 1.1, SUPERBEE 1.47, auto, 256x32).

Figures 13a through 13h display the results using the k-ω 2006 turbulence model with the stress limiter weight increased from its standard value to 1.1. The far-field turbulence intensity was set to 0.5%. The simulation was unstable with a far-field turbulence intensity of 0.05%. The final values of y^+ based on cell height next to the airfoil at an AOA of 23 vary from 15 to 0.19.

The plot of lift and drag only goes to 23 degrees because the k-ω 2006 turbulence model was less stable than the SST model at 24 degrees AOA. The grid is the same as that used with the SST turbulence model for a chord of two feet except that the vertical grid-layer size is increased to $2x10^{-4}$ m. The fit to experiment is similar to that obtained using the SST turbulence model. The match between airfoil forces at Reynolds numbers $3x10^6$ and $6x10^6$ is much better than obtained using the SST turbulence model. Halving or doubling the value of vertical grid-layer size reduces the fit to experiment for high values of AOA below 18 degrees.

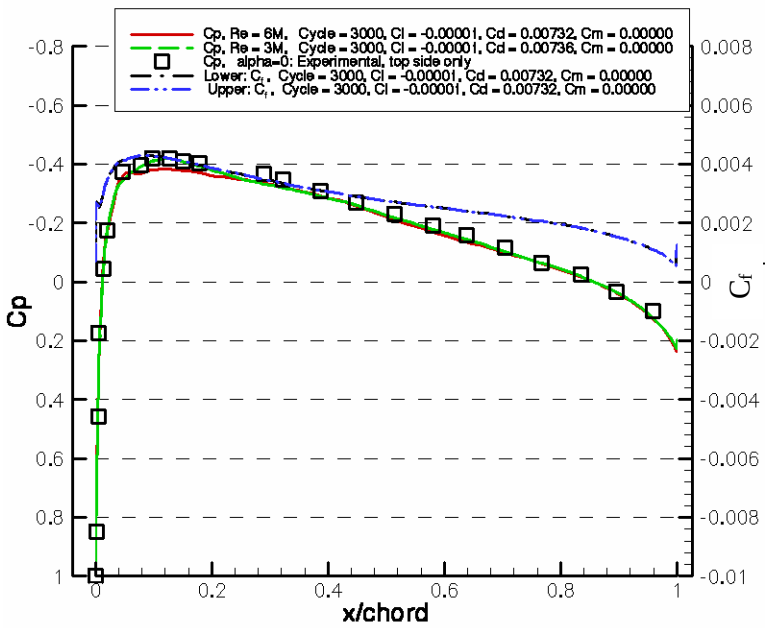

Fig. 13c: Cp & C_f, AOA = 0 (k-ω 2006, Lim = 1.1, SUPERBEE 1.47, auto, 256x32).

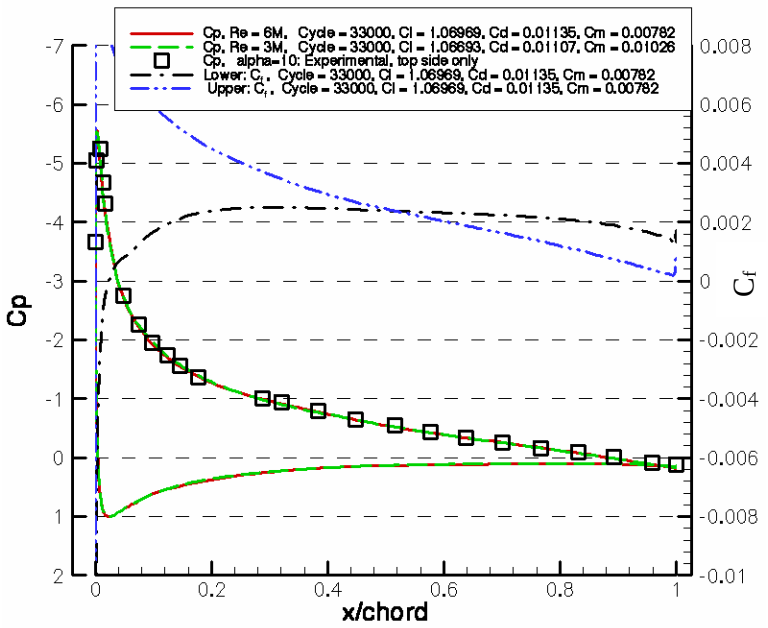

Fig. 13d: Cp & C_f, AOA = 10 (k-ω 2006, Lim = 1.1, SUPERBEE 1.47, auto, 256x32).

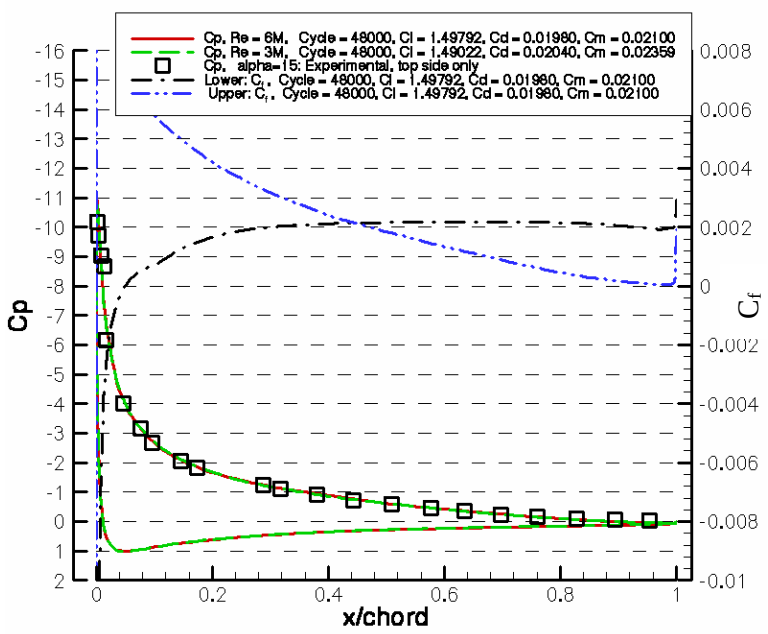

Fig. 13e: Cp & C_f, AOA = 15 (k-ω 2006, Lim = 1.1, SUPERBEE 1.47, auto, 256x32).

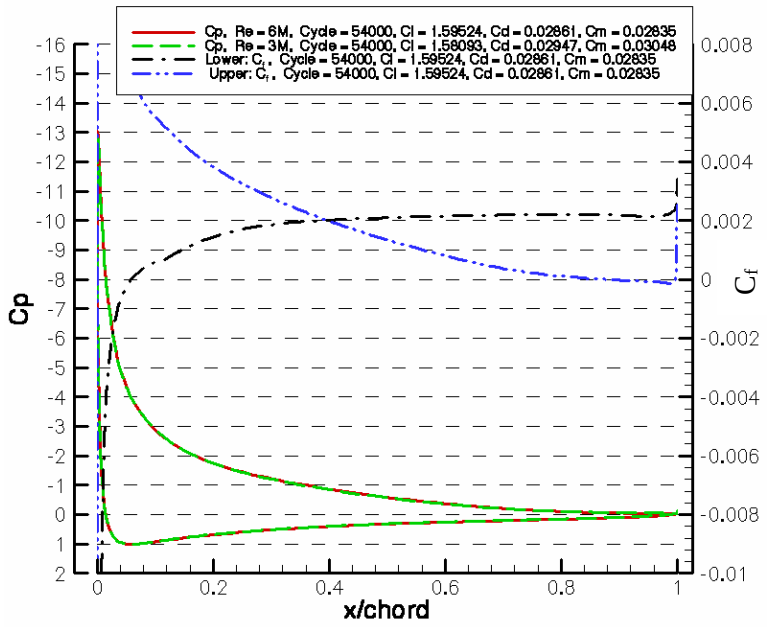

Fig. 13f: Cp & C_f, AOA = 17 (k-ω 2006, Lim = 1.1, SUPERBEE 1.47, auto, 256x32).

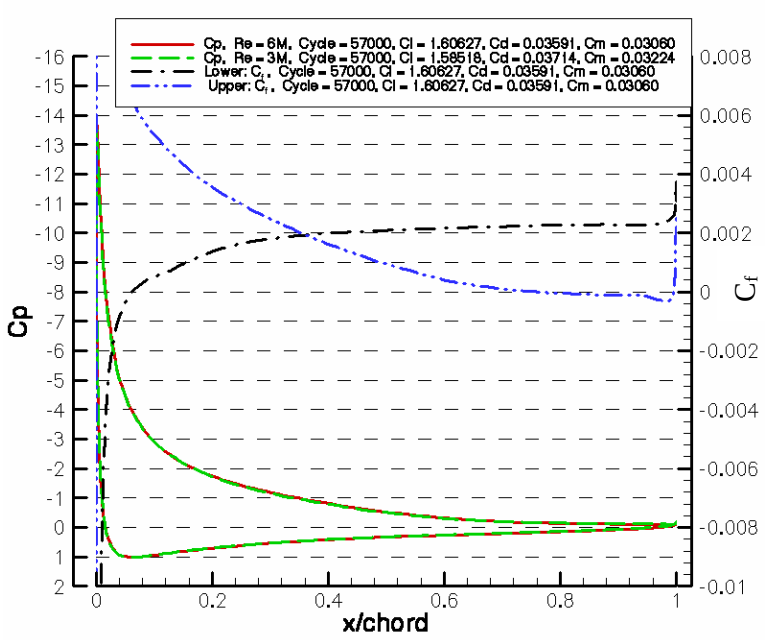

Fig. 13g: Cp & C_f, AOA = 18 (k-ω 2006, Lim = 1.1, SUPERBEE 1.47, auto, 256x32).

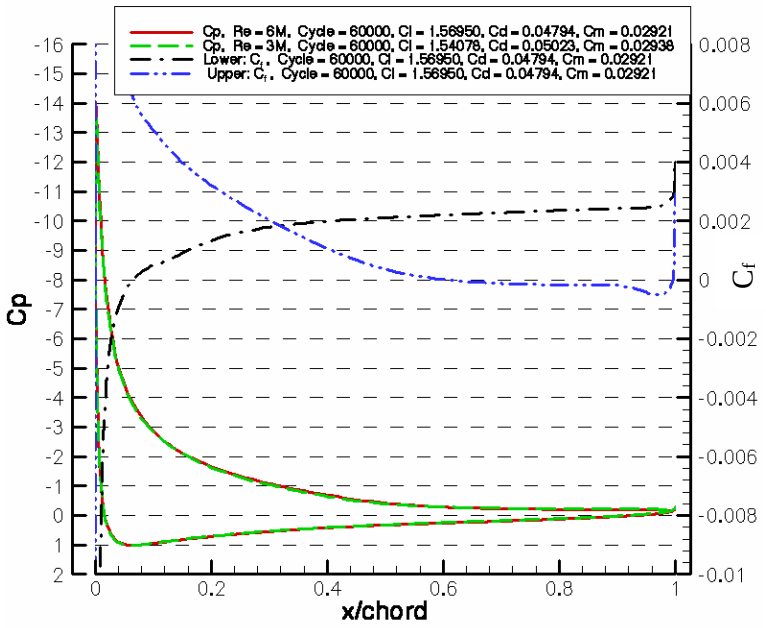

Fig. 13h: Cp & C_f, AOA = 19 (k-ω 2006, Lim = 1.1, SUPERBEE 1.47, auto, 256x32).

The simulation was repeated using a 512x32 grid and resulted in the same stall angle and a similar fit to experiment. A simulation using a 128x32 cell grid resulted in a stall angle near 16 degrees AOA and a poor fit to experimental values of lift and drag above 13 degrees AOA.

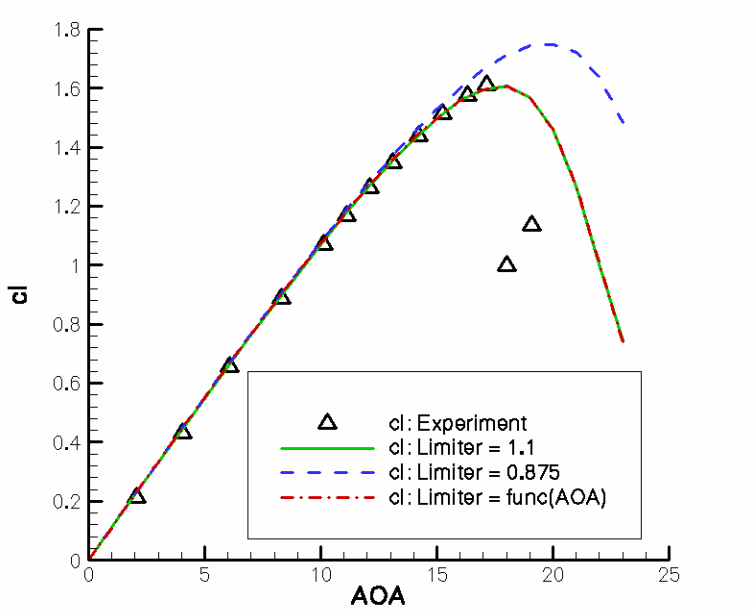

Fig. 14a: Lift versus AOA (k-ω 2006, SUPERBEE 1.47, auto, 256x32).

Figure 14a displays plots of lift versus AOA with the stress limiter weight set to 1.1 and to 0.875. Also shown is a curve where the stress limiter weight is 0.875 at AOA 0 degrees and increases slowly and then quickly in a nonlinear manner until it reaches 1.1 at AOA 15 degrees. All the curves coincide until about AOA 13 degrees when the curve corresponding to a stress limiter weight of 0.875 starts to depart from the experimental values.

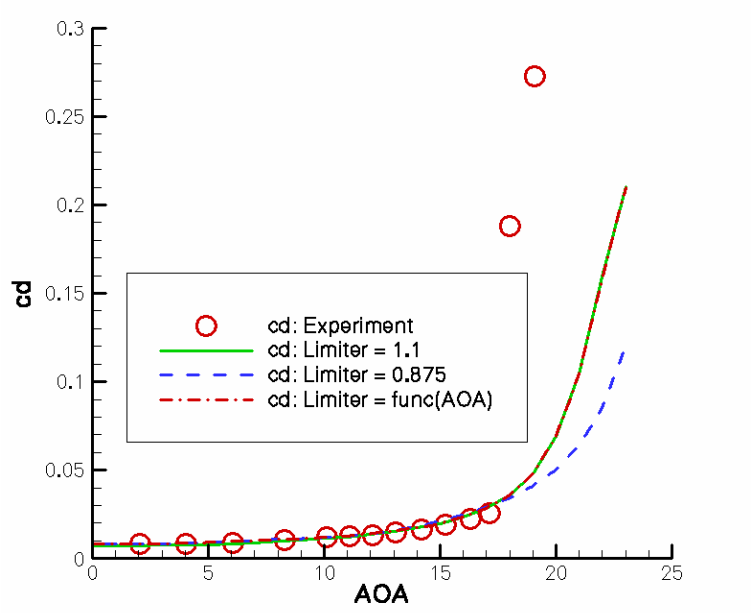

Fig. 14b: Drag versus AOA (k-ω 2006, SUPERBEE 1.47, auto, 256x32).

In Figure 14b, All the drag curves from simulation appear to coincide until about AOA 18 degrees where the curve corresponding to a stress limiter weight of 0.875 starts to depart from the other curves.

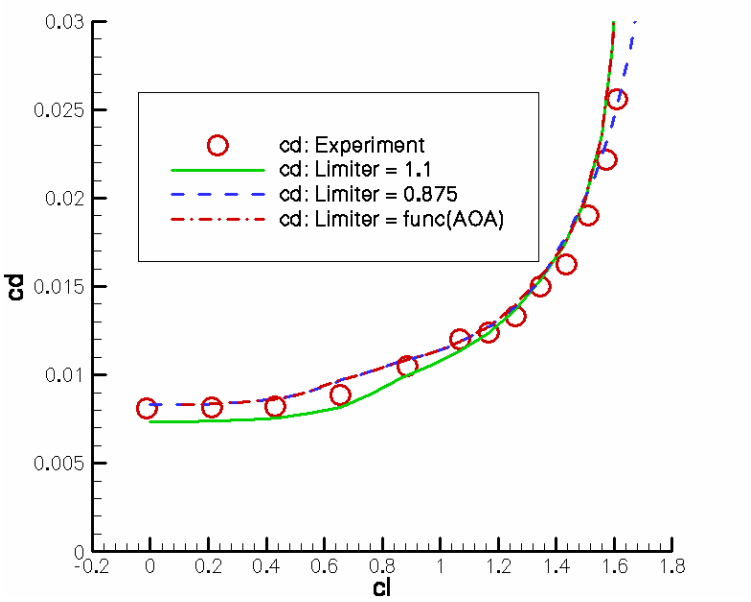

Fig. 14c: Drag versus lift (k-ω 2006, SUPERBEE 1.47, auto, 256x32).

However, as shown in the plots of drag versus lift in Figure 14c, there is a visible difference in drag for small values of AOA. The curves with differing values of stress limiter weight merge at about 13 degrees AOA. One might be tempted to use a value intermediate between 0.875 and 1.1 at low AOA. However, as shown in Figure 14d, the best fit to experimental values of pitching moment up to AOA 16 degrees is obtained with the stress limiter weight set to 0.875.

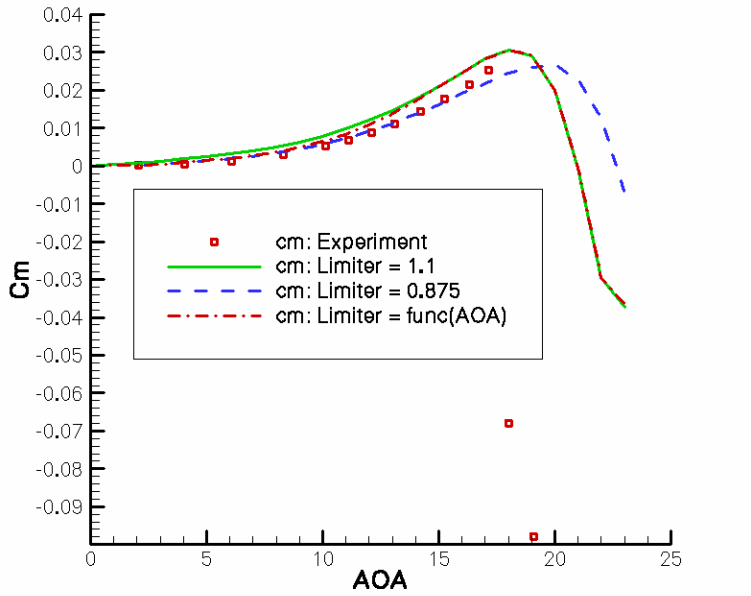

Fig. 14d: Cm versus AOA (k-ω 2006, SUPERBEE 1.47, auto, 256x32).

4.1 *Aerodynamic Center and Pitching-Moment Curves*

All the NACA 0012 simulations are performed with the aerodynamic center set to the quarter chord point. The pitching moment is positive and increases with angle of attack in a manner consistent with the data of Ladson [5] who also sets the aerodynamic center to the quarter chord point.

The aerodynamic center is typically defined as the point about which the pitching moment does not change with angle of attack. More practically, the aerodynamic center may be defined as the point at which the pitching moment is almost constant over a substantial range of angle of attack. This can be seen by examining the pitching moment plots in Abbott and von Doenhoff [7], where the pitching moment coefficient departs from a nearly constant value as maximum lift is approached. Knowledge of the aerodynamic center is important in analyzing the longitudinal stability of an aircraft. Standard inviscid flow analysis for thin symmetric airfoils at small angles of attack locate the aerodynamic center at the quarter chord point. More advanced analysis shows that this is only approximately correct.

EasyFlowfield outputs a series of estimates of the aerodynamic center as AOA is increased or decreased. Use of the aerodynamic center output for a particular value of AOA typically results in a reduced change in Cm between the initial AOA and that AOA.

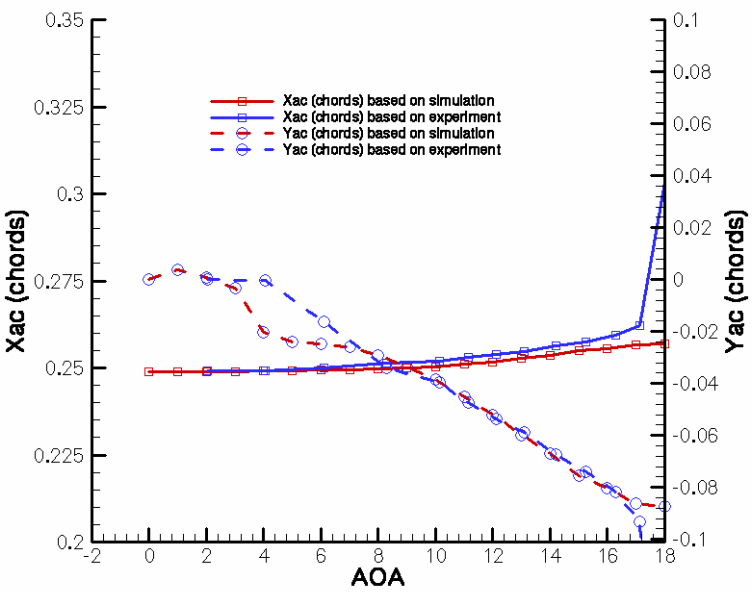

Fig. 15: Estimates of aerodynamic center at various values of AOA (Lim = func(AOA).

Figure 15 displays estimates of the aerodynamic center for various values of AOA obtained from the k-ω 2006 simulation with variable stress limiting. Also shown are estimates of aerodynamic center obtained by analysing the values of Cl, Cd, and Cm from the measurements of Ladson [5]. There is reasonable agreement in the estimates from simulation and experiment at higher values of AOA until the condition of stall is approached. The simulation was started at an AOA of -1 degrees to allow estimation of the aerodynamic center at zero degrees AOA. Two points were taken out of the experimental data, so it started at 0.05 degrees AOA instead of -4.04 degrees AOA

EasyFlowfield created restart files during the simulation. The restart files were used to efficiently repeat output of the aerodynamic force coefficients as a function of AOA with different aerodynamic centers. This output was used to create the following figures.

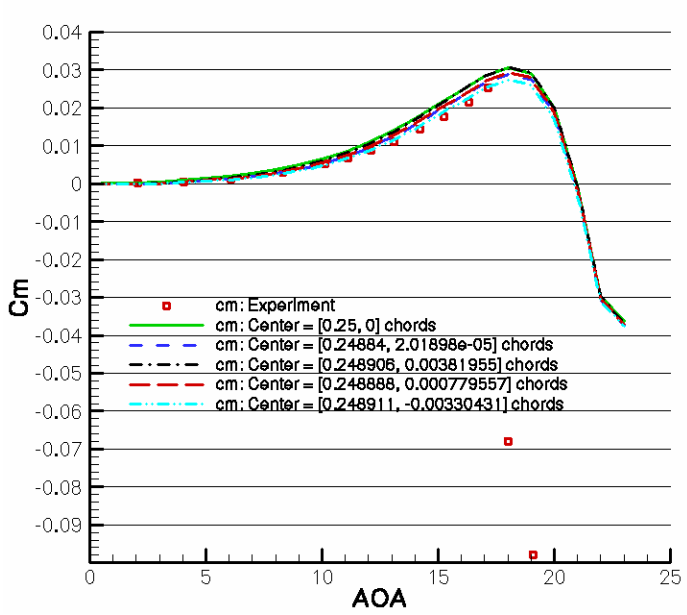

Fig. 16: Cm versus AOA (k-ω 2006, Lim = func(AOA), SUPERBEE 1.47, auto, 256x32).

Figure 16 displays plots of pitching moment versus AOA. In addition to the experimental points and a plot of Cm with the aerodynamic center set to the quarter chord point, plots using the aerodynamic center estimated at 0-, 1-, 2-, and 3-degrees AOA are included. The best fit to the experimental points was obtained using the estimate at 3 degrees AOA.

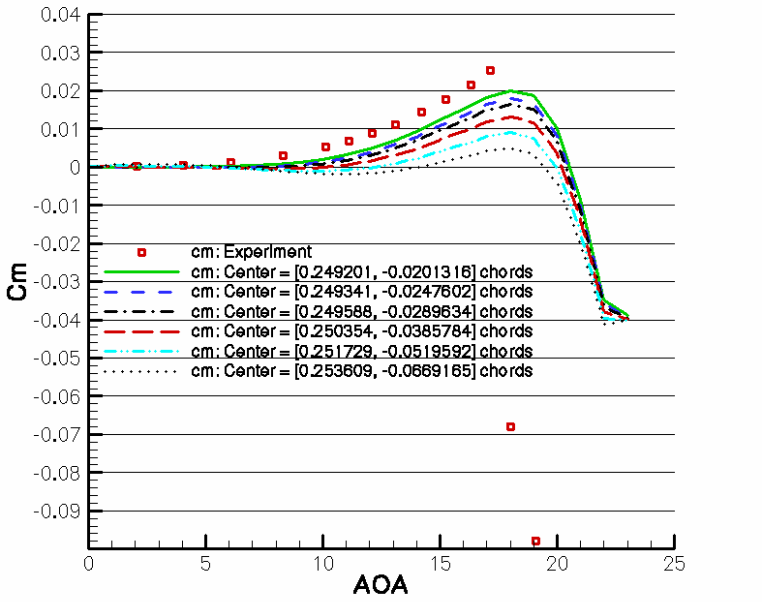

Fig. 17: Cm versus AOA (k-ω 2006, Lim = func(AOA), SUPERBEE 1.47, auto, 256x32).

However, it is most desirable to use an aerodynamic center where Cm remains almost constant over a broad range of AOA. Figure 17 displays the experimental points with Cm curves using the aerodynamic centers estimated at 4-, 6-, 8-, 10-, 12- and 14-degrees AOA. The widest range of Cm with nearly constant Cm was obtained using the estimate at 12 degrees AOA. The curve of Cm obtained using the estimate at 14 degrees AOA displays a significant undulation but may be deemed acceptable or desirable by some designers.

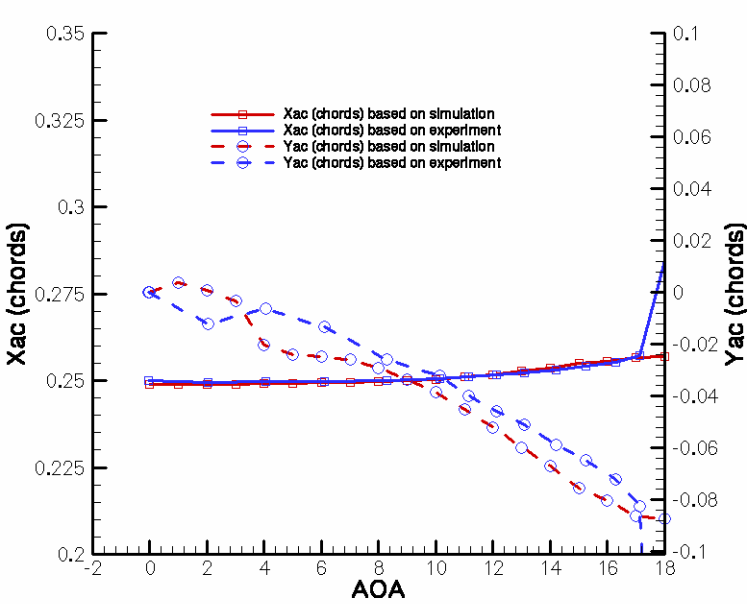

Fig. 18a: Estimates of aerodynamic center at various values of AOA (Lim = func(AOA)) using tripped transition experimental data starting at -2.14 degrees AOA.

As noted above, two points are absent from the experimental data, so that it starts at 0.05 degrees AOA instead of -4.04 degrees AOA. If -2.14 degrees AOA is included, the Xac curves shown in Figure 18a are then almost identical to each other, but the experimental Yac curves are displaced upwards. The aerodynamic centers based on the extended experimental forces are still well matched by the aerodynamic centers based on simulation. Figure 18b shows a slightly better match to experiment when the simulation AOA is started at -2 degrees and incremented in steps of two degrees.

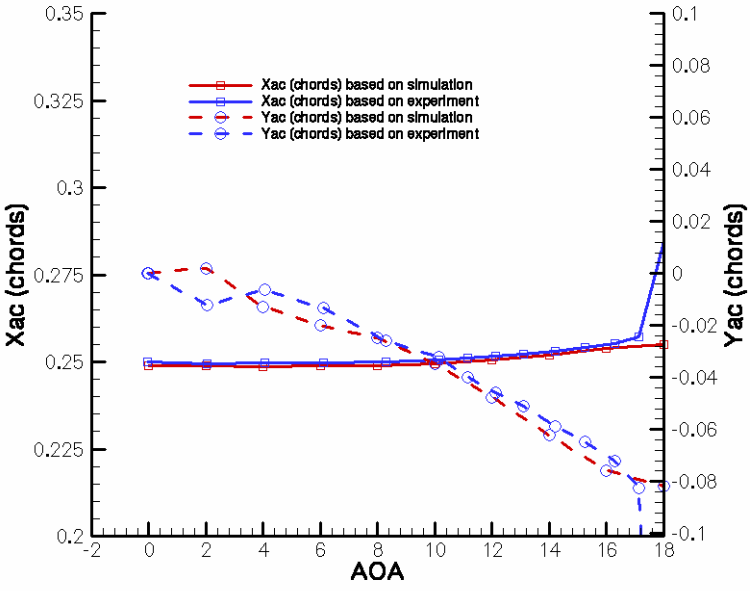

Fig. 18b: Estimates of aerodynamic center at various values of AOA (Lim = func(AOA), ΔAOA = 2) using tripped transition experimental data starting at -2.14 degrees AOA.

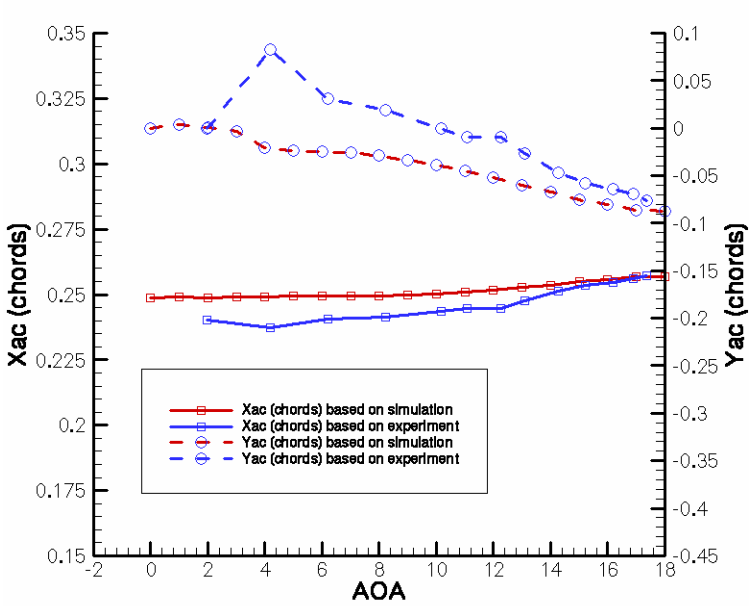

Fig. 19: Estimates of aerodynamic center at various values of AOA (Lim = func(AOA)) using free transition experimental data starting at 0.05 degrees AOA.

As previously indicated, the measurements were performed with forced transition. As shown in Figures 19 and 20, measurements performed with free transition by Ladson [5] do not result in such a close agreement of the aerodynamic center estimates. The aerodynamic center curves produced using airfoil forces with free transition are not as smooth as the aerodynamic center curves produced from tripped airfoil forces.

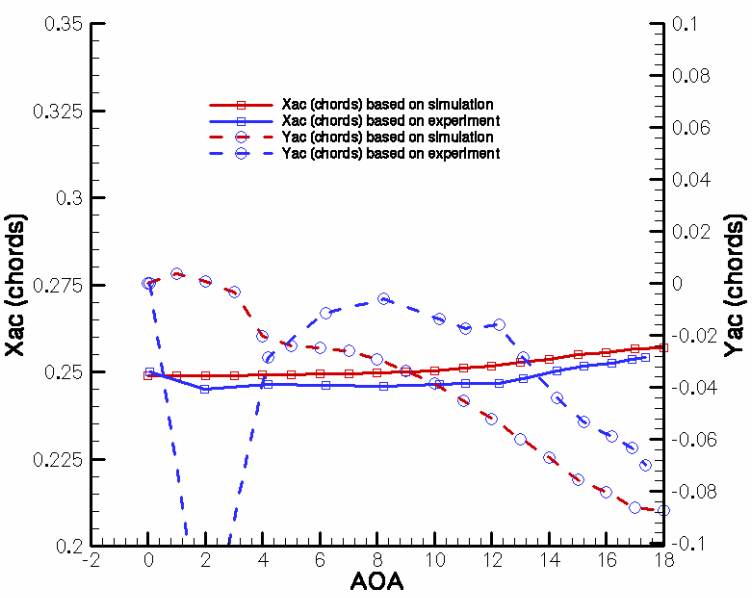

Fig. 18e: Estimates of aerodynamic center at various values of AOA (Lim = func(AOA)) using free transition experimental data starting at -2 degrees AOA.

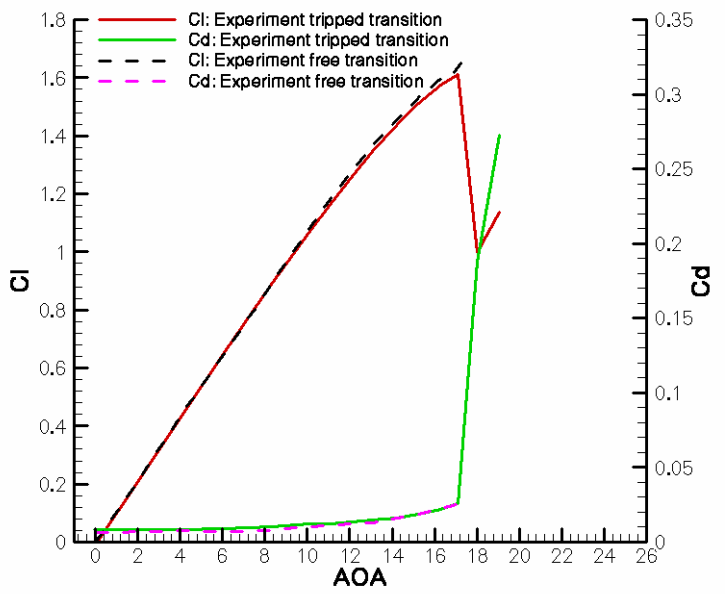

Fig. 21a: Experimental Cl and Cd vs AOA for tripped and free transition (Ladson [5]).

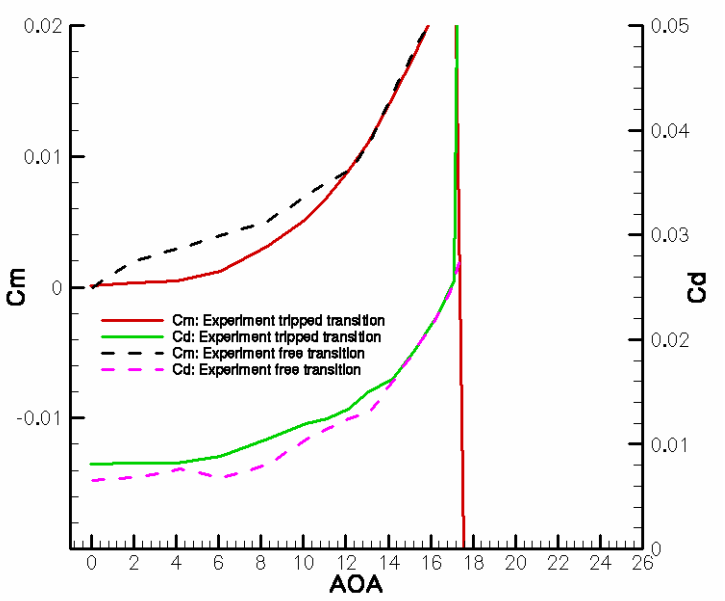

Fig. 21b: Experimental Cm and Cd vs AOA for tripped and free transition (Ladson [5]).

As seen in Figure 21, most of the irregularity is due to the pitching moment and drag forces. The point of transition approaches the leading-edge at large values of AOA but is not a smooth function of AOA at lower values of AOA.

A turbulence model with a robust and accurate transition model, available in a simulation code other than EasyFlowfield, might reproduce the irregular drag and pitching moment curves. Note that the output of this hypothetical simulation code can be analysed by EasyFlowfield to potentially replicate the aerodynamic center curves for free transition. The hypothetical simulation code can be used to evaluate the predicted aerodynamic centers. However, due to the variability of the aerodynamic center curves, it may be difficult to determine an aerodynamic center much better than the traditional value of [0.25, 0] chords for an airfoil with free transition. The aerodynamic center predictions produced by EasyFlowfield should be more useful for aircraft designs using tripped transition.

References

[1] Cook, P. H., McDonald, M. A., Firmin, M. C. P., "Aerofoil RAE 2822 - Pressure Distributions, and Boundary Layer and Wake Measurements," in Experimental Data Base for Computer Program Assessment, AGARD Report AR 138, 1979.

[2] Holst, T. L., Viscous Transonic Airfoil Workshop Compendium of Results, AIAA-87-1460, 1987.

[3] Wilcox, D. C., Turbulence Modeling for CFD, 3rd ed., DCW Industries Inc., 2006.

[4] Bardina, J. E., Huang, P. G., Coakley, T. J., Turbulence Modelling Validation, Testing, and Development, NASA TM 110446, 1997.

[4] Menter, F. R., Improved two-equation k-ω Turbulence Models for Aerodynamic Flows, NASA TM-103975, 1992.

[5] Ladson, C. L., Effects of Independent Variation of Mach and Reynolds Numbers on the Low-Speed Aerodynamic Characteristics of the NACA 0012 Airfoil Section, NASA TM-4074, 1988.

[6] Gregory, N., O'Reilly, C. L., Low-Speed Aerodynamic Characteristics of NACA 0012 Aerofoil Section, including the Effects of Upper-Surface Roughness Simulating Hoar Frost, R. & M. No. 3726, 1973.

[7] Abbott, I. H., von Doenhoff, A. E., Theory of Wing Sections; Including a Summary of Airfoil Data, Dover Publications, New York, 1959.